Journal of The Electrochemical Society, **156** (3) A246-A252 (2009)
0013-4651/2009/156(3)/A246/7/$23.00 © The Electrochemical Society

Electrochemical Behavior of $LiM_{0.25}Ni_{0.25}Mn_{1.5}O_4$ as 5 V Cathode Materials for Lithium Rechargeable Batteries

S. Rajakumar,[a] R. Thirunakaran,[a] A. Sivashanmugam,[a] Jun-ichi Yamaki,[b,*] and S. Gopukumar[a,z]

[a]*Central Electrochemical Research Institute, Karaikudi-630 006, Tamil Nadu, India*
[b]*Institute for Materials Chemistry and Engineering, Kyushu University, Kasuga 816-8580, Japan*

Glycine-assisted sol-gel–synthesized multiple-doped spinels, $LiM_{0.25}Ni_{0.25}Mn_{1.5}O_4$ (M = Cr, Fe, and Co) have been studied as 5 V cathode materials. The sol-gel technique provides homogeneity, high purity, lower processing temperature, controlled particle size, and morphology. The synthesized samples were subjected to physical characterization studies, viz., thermogravimetric and differential thermal analysis, X-ray diffraction, scanning electron microscopy, X-ray photoelectron spectroscopy, and electrochemical charge–discharge studies. Galvanostatic charge–discharge studies of the samples reveal that $LiFe_{0.25}Ni_{0.25}Mn_{1.5}O_4$ using glycine as a chelating agent delivers a stable capacity of 120 mAh g^{-1} even after 20 cycles when cycled between 3 and 5 V.
© 2009 The Electrochemical Society. [DOI: 10.1149/1.3071364] All rights reserved.

Manuscript submitted August 14, 2008; revised manuscript received December 17, 2008. Published January 29, 2009.

Material innovation and systematic research paved the way for the development of transition metal oxides, viz., $LiCoO_2$, $LiNiO_2$, and $LiMn_2O_4$ as cathode materials for rechargeable lithium batteries. Furthermore, replacement of $LiCoO_2$ has been actively attempted by using less toxic manganese-based cathode materials for obtaining high-voltage cycling.[1] Among the three compounds, $LiMn_2O_4$ is an attractive cathode material owing to its ease of synthesis, low cost, abundance, environmentally benign nature, improved safety, and good reversibility. Despite its advantages, the capacity of the pure spinel $LiMn_2O_4$ upon repeated cycling diminishes at elevated temperature.[2] The capacity fade has been attributed to Jahn–Teller distortion,[3] two-phase unstable reaction,[4] slow dissolution of manganese into the electrolyte,[5] particle disruption, and lattice instability.[6,7] In an ideal case, Jahn–Teller active Mn^{3+} ions should not be present to avoid the structural and chemical instabilities by partially substituting manganese with metal cations thereby enhancing the structural stability. Ohzuku et al.[8] substituted manganese with 3d transition metals such as Co, Cr, Cu, Ni, Ti, Zn, and Fe in $LiMn_2O_4$, and the most remarkable property of these kinds of materials are their higher discharge plateaus of >4 V. The high working voltage can lead to a high power density; thus, the batteries with these materials as cathode will produce higher power output. Lee et al.[9] investigated the degradation mechanism in doped $LiMn_2O_4$. Among the different dopants, Ni^{2+} ions are found to be beneficial in stabilizing the spinel structure and also make it as 5 V cathode materials as Ni^{2+}/Ni^{4+} transition occurs above 4.79 V.[10] However, Ni-doped $LiMn_2O_4$ suffers substantial degradation in the electrochemical performance mainly due to structural and chemical instabilities resulting from the high-spin Mn^{3+} ions, which is closely related with the oxygen deficiency of the spinel compound during the heat-treatment process at high temperatures. Furthermore, it has been observed that all Mn^{3+} are not substituted by Ni^{2+} ions, but a small fraction of Mn^{3+} is usually observed in these compounds even after the heat-treatment at high temperatures. In order to restrain the formation of Mn^{3+} due to oxygen deficiency at high temperatures, the researchers correlated the bond dissociation energies between transition metal (M) and oxygen (O) ions in the compound. The greater the M–O bond energies than that of Mn–O bond make the material structurally stable with enhanced electrochemical activity. This could be achieved by appropriate double doping with elements such as chromium, iron, and cobalt, which have larger bonding energy than that of Mn–O.[11-16] Hwang et al.[17] and Tsai et al.[18] have reported better cycling performance for Co^{3+} and Ni^{2+} spinel $LiMn_2O_4$ compared to the undoped one. Furthermore, the materials prepared by the low-temperature sol-gel method possess less impurity, small particle size with homogeneous size distribution, and controlled morphology in contrast to that by the traditional solid-state reaction. In the present investigation, the physical and electrochemical characteristics of duo doped $LiM_{0.25}Ni_{0.25}Mn_{1.5}O_4$ (M = Fe, Cr, Co) are studied as a possible 5 V cathode material.

Experimental

Figure 1 shows the flow chart for the synthesis of spinel $LiM_{0.25}Ni_{0.25}Mn_{1.5}O_4$ (M = Fe, Cr, Co) by a sol-gel method using glycine as a chelating agent. Stoichiometric amounts of high-purity nitrates of lithium, manganese, nickel with either cobalt, iron, or chromium nitrate were uniformly mixed and dissolved in triple-distilled water. The solution was stirred continuously with gentle heating, and 1 M glycine was added as a chelating agent to get a homogeneous solution. A viscous gel was obtained, and the pH was maintained between 5 and 7. The gel mass was dried in a hot air oven at 110°C. A portion of the gel precursor was characterized by thermogravimetric and differential thermal analysis [(TG/DTA), PL Thermal Sciences instrument model STA 1500] to ascertain the thermal behavior. The dried mass was ground well and calcined at different temperatures, viz., 250, 400, 600, and 850°C, for 8 h in alu-

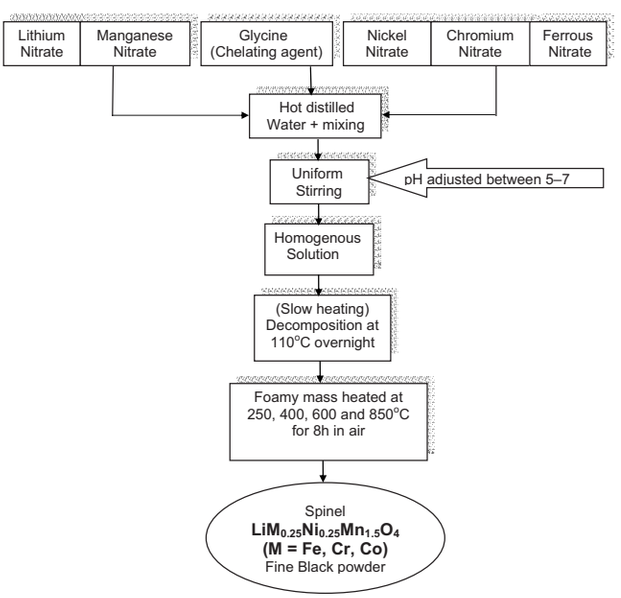

Figure 1. Flow chart for the synthesis of spinel $LiM_{0.25}Ni_{0.25}Mn_{1.5}O_4$ (M = Cr, Fe, and Co) by sol-gel method using glycine as a chelating agent.

* Electrochemical Society Active Member.
z E-mail: deepika_41@rediffmail.com

Downloaded 30 Jun 2009 to 210.212.252.226. Redistribution subject to ECS license or copyright; see http://www.ecsdl.org/terms_use.jsp

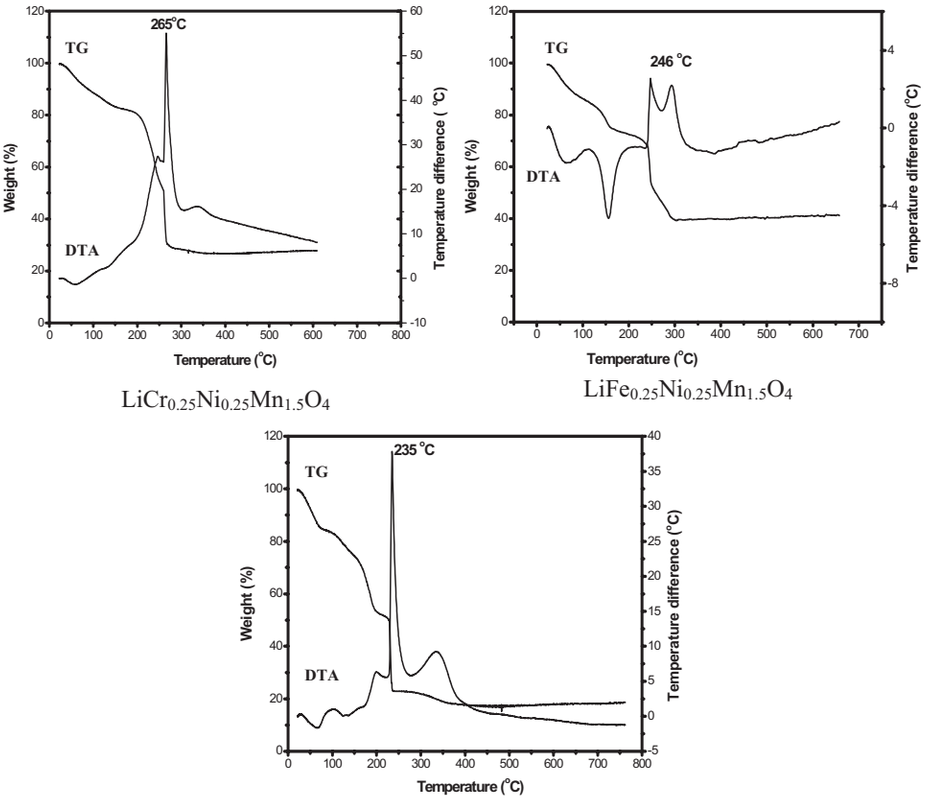

Figure 2. TG/DTA analysis of spinel $LiM_{0.25}Ni_{0.25}Mn_{1.5}O_4$ (M = Cr, Fe, and Co) precursors.

mina crucibles and subjected to physical and electrochemical characterization. Powder X-ray diffraction (XRD) studies were made on a JEOL JDX-8030 X-ray diffractometer with nickel-filtered Cu Kα radiation between scattering angles of 15 and 80°. Morphological features of the products were examined using a Hitachi S-3000 H scanning electron microscope.

Electrochemical cell assembly.— The electrochemical cell was a typical 2016 coin cell (Hohsen Co., Japan) assembled in an argon-filled glove box (MBraun, Germany) using lithium foil as the anode, Celgard 2400 as the separator, and 1 M solution of $LiPF_6$ in 50:50 (v/v) mixture of ethylene carbonate (EC) and diethylene carbonate (DEC) as the electrolyte. The cathode was prepared by a slurry-coating procedure. The cathode slurry consisted of 85% of the synthesized material, 10% conducting carbon, and 5% poly vinylidiene fluoride binder dissolved in n-methyl-2-pyrrolidone. The slurry was coated over aluminum foil and vacuum dried at 110°C for 2 h. The dried coating was pressed under 10 tons load for 2 min, and blanks of 18 mm diam were punched out and used as cathode. These coin cells were used for charge–discharge cycling and also for cyclic voltammetry (CV) studies. The charge–discharge cycling studies were carried out at a constant current of C/10 rate between 3 and 5 V in a battery cycling unit. CV of $LiFe_{0.25}Ni_{0.25}Mn_{1.5}O_4$ electrodes were performed at a scan rate of 10 $\mu V\ s^{-1}$ in the potential range of 3.0–5.0 V using a PAR 273A (EG&G) potentiostat. Lithium foil was used as the reference and counter electrode, $LiFe_{0.25}Ni_{0.25}Mn_{1.5}O_4$ electrode as the working electrode, and 1 M solution of $LiPF_6$ in 50:50 (v/v) mixture of EC and DEC as the electrolyte.

X-ray photoelectron spectroscopy (XPS) of the synthesized powder was investigated using VG electron spectroscope. The powder sample was made as a pallet and affixed to the sample holder. All spectra were recorded using an X-ray source (Al Kα radiation) with a scan range of 0–1200 eV binding energy. The collected high-resolution XPS spectra were analyzed using an XPS peak software fitting program. The energy scale was adjusted on the carbon peak in C 1s spectra at 284.9 eV.

Results and Discussion

TG/DTA studies.— Figures 2a-c depict TG/DTA curves of spinel $LiM_{0.25}Ni_{0.25}Mn_{1.5}O_4$ doped with Cr, Fe, and Co, respectively. In the case of $LiCr_{0.25}Ni_{0.25}Mn_{1.5}O_4$ (Fig. 2a) two weight-loss zones are observed. The first weight-loss zone (18%) extending up to 180°C is accounted for the elimination of moisture. Subsequently, the second weight-loss (52%) region observed between 180 and 265°C corresponds to the decomposition of nitrate precursors. The decomposition reaction is depicted as a sharp exothermic peak in the DTA curve centered at 265°C, which is lower than the undoped one, indicating the earlier formation of $LiCr_{0.25}Ni_{0.25}Mn_{1.5}O_4$.

In the case of $LiFe_{0.25}Ni_{0.25}Mn_{1.5}O_4$ (Fig. 2b), two weight-loss zones are also observed. The first weight-loss zone (62%) coupled with double endothermic events observed up to 230°C can be attributed to the removal of water molecules and ammonia gas. Furthermore, the two exothermic peaks obtained around 246 and 296°C could be associated with 62% weight loss and vindicate the formation reaction of the spinel product.

TG/DTA curves of $LiCo_{0.25}Ni_{0.25}Mn_{1.5}O_4$ (Fig. 2c) indicate stepwise weight-loss zones corresponding to two small exothermic peaks at 100 and 200°C corresponding to initial elimination of moisture (15%), and a sharp exothermic peak centered at 235°C followed by a shallow exothermic peak of ~335°C amounting to 68% weight loss are assignable to the decomposition of nitrate precursors and the formation of the spinel product. An overall reduction in the formation temperature from the pristine spinel may be attributed to the higher specific heat of the Cr, Fe, and Co precursors.

XRD.— Figure 3 illustrates the XRD profiles of sol-gel synthesized $LiM_{0.25}Ni_{0.25}Mn_{1.5}O_4$ (M = Cr, Fe, and Co), respectively, us-

Downloaded 30 Jun 2009 to 210.212.252.226. Redistribution subject to ECS license or copyright; see http://www.ecsdl.org/terms_use.jsp

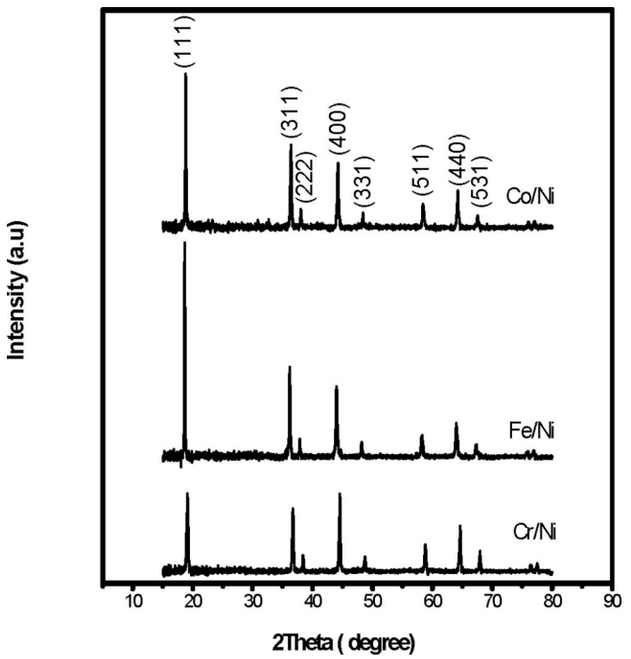

Figure 3. XRD patterns of $LiM_{0.25}Ni_{0.25}Mn_{1.5}O_4$ (M = Cr, Fe, and Co) samples calcined at 850°C.

ing glycine as a chelating agent calcined at 850°C. All the peak reflections perfectly match with JCPDS card no. 35-782, corresponding to the spinel compound. Spectral profiles of Cr/Ni-, Fe/Ni-, and Co/Ni-doped spinels exhibit a high degree of crystallinity and better phase purity. The peaks corresponding to (111), (311), (222), (400), (331), (551), (440), and (531) planes hold a striking similarity to that of the previous researchers.[19-21] The high-intensity peaks corresponding to the planes (111), (311), and (400) confirm the occupancy of lithium ions in tetrahedral 8a sites, and the manganese ions in 16d sites and O^{2-} ions in 32e sites.[22-24] Table I shows the crystallite size obtained from the Debye–Scherrer formula for $LiM_{0.25}Ni_{0.25}Mn_{1.5}O_4$ (M = Cr, Fe, and Co) compounds, and unit cell parameters have been calculated from XRD data. It can be seen that all the compounds prepared exhibit an average crystallite size of ~60 nm.

Table I. Unit cell parameters and crystallite size of $LiM_{0.25}Ni_{0.25}Mn_{1.5}O_4$ (M = Cr, Fe, Co) compounds.

No.	Sample	*a* (Å)	Unit cell volume $(Å)^3$	Crystallite size $\times 10^{-9}$ m
1	$LiCr_{0.25}Ni_{0.25}Mn_{1.5}O_4$	8.230	557	60.20
2	$LiFe_{0.25}Ni_{0.25}Mn_{1.5}O_4$	8.229	555	60.23
3	$LiCo_{0.25}Ni_{0.25}Mn_{1.5}O_4$	8.225	551	60.25

SEM.— Figures 4a-c depict scanning electron microscopy (SEM) images of $LiM_{0.25}Ni_{0.25}Mn_{1.5}O_4$ (M = Cr, Fe, and Co) powders calcined at 850°C, respectively. The particles of $LiCr_{0.25}Ni_{0.25}Mn_{1.5}O_4$ (Fig. 4a) are present as larger grains of average particle size around 1 μm with clear grain boundaries. $LiFe_{0.25}Ni_{0.25}Mn_{1.5}O_4$ particles (Fig. 4b) appear as agglomerated and are smaller than that of Cr-doped and the average grain size ranging from 0.5 to 1 μm size. In the case of $LiCo_{0.25}Ni_{0.25}Mn_{1.5}O_4$ (Fig. 4c) a majority of the particles are <0.5 μm and few particles are of 1 or 2 μm in size.

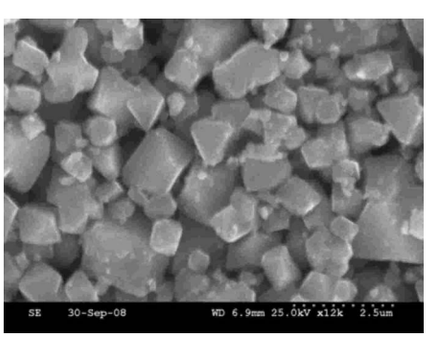

(a) $LiCr_{0.25}Ni_{0.25}Mn_{1.5}O_4$

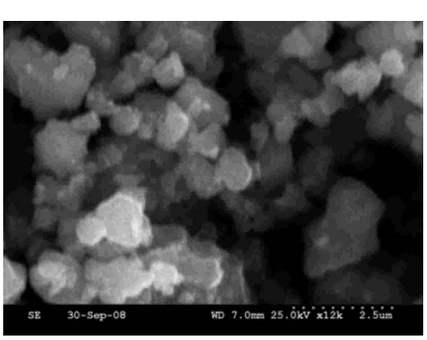

(b) $LiFe_{0.25}Ni_{0.25}Mn_{1.5}O_4$

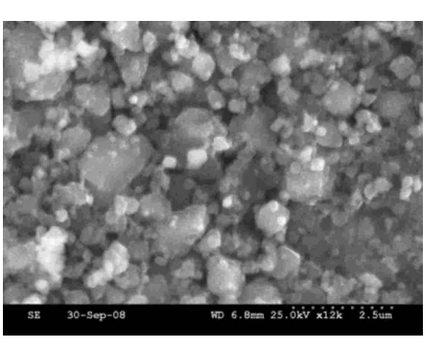

(c) $LiCo_{0.25}Ni_{0.25}Mn_{1.5}O_4$

Figure 4. SEM images of $LiM_{0.25}Ni_{0.25}Mn_{1.5}O_4$ (M = Cr, Fe, and Co) samples calcined at 850°C.

Downloaded 30 Jun 2009 to 210.212.252.226. Redistribution subject to ECS license or copyright; see http://www.ecsdl.org/terms_use.jsp

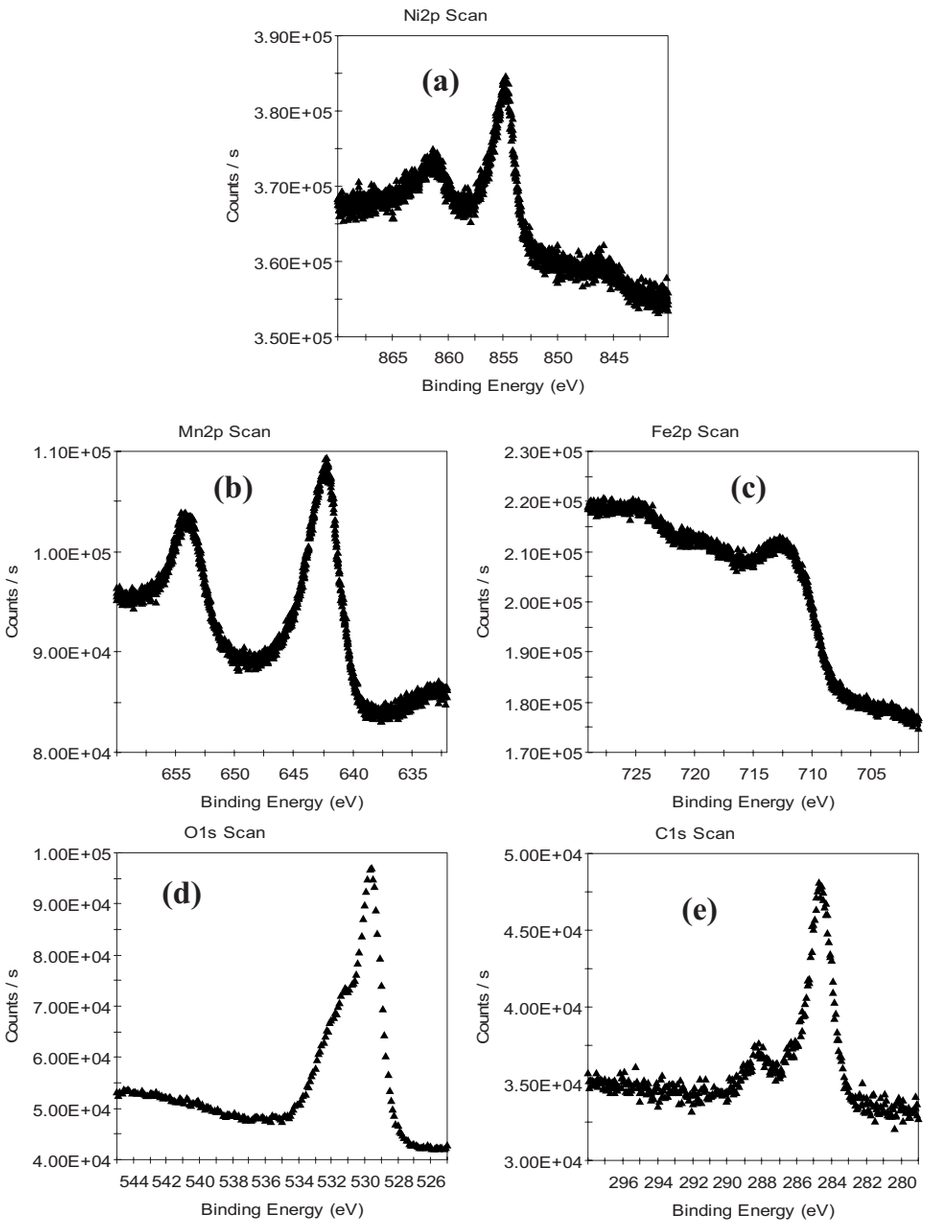

Figure 5. XPS of $LiFe_{0.25}Ni_{0.25}Mn_{1.5}O_4$.

XPS studies.— XPS studies of $LiFe_{0.25}Ni_{0.25}Mn_{1.5}O_4$ powder have been carried out to elucidate the oxidation states of the metal species present in the spinel compound and are depicted in Fig. 5a-c. The binding energies in the XPS spectrum located at ~855 eV with a satellite peak at 862 eV in Fig. 5a could be assigned to Ni^{2+}. Similar observations have been reported by other researchers, and the satellite peak has been assigned due to the multiple splitting of nickel oxide energy levels.[25-27] Figure 5b represents the XPS spectra of Mn 2p. A major peak located at the binding energy of ~642.5 eV, which can be attributed to Mn^{4+}, and the satellite peak observed at ~654 eV are in agreement with the literature values.[27,28] Figure 5c indicates the XPS spectra of Fe 2p. The binding energy peak located at ~711 eV, which can be attributed to Fe^{3+}, and the satellite peak observed at ~725 eV are in agreement with that of Hernan et al.[29] Furthermore, the binding energy O 1s is located at ~529.8 eV (Fig. 5d) and C 1s binding energy is observed at ~285 eV in the present XPS measurements (Fig. 5e) originating from oxygen linked to Mn–O and Ni–O and Fe–O in the synthesized material.

Charge–discharge studies.— First charge–discharge cycle and cycling behavior of $LiM_{0.25}Ni_{0.25}Mn_{1.5}O_4$ (M = Cr, Fe, and Co) calcined at 850°C are shown in Fig. 6a-c and 7a-c, respectively. $LiCr_{0.25}Ni_{0.25}Mn_{1.5}O_4$ delivers 116 mAh g^{-1} against the charging capacity of 154 mAh g^{-1} during the first cycle. The performance realized in the case of chromium-doped spinel may be ascribed to the low order of cation mixing and higher octahedral stabilization energy of chromium (i.e., 1142 kJ $mole^{-1}$) as compared to that of manganese (i.e., 946 kJ $mole^{-1}$), which ensures the stabilization of the spinel structure. Furthermore, these results are superior than the earlier one,[30] wherein $LiCr_{0.10}Ni_{0.40}Mn_{1.5}O_4$ delivered discharge capacity of only 111 mAh g^{-1} during the first cycle. Even though, $LiCr_{0.25}Ni_{0.25}Mn_{1.5}O_4$ cells experience a fading trend up to the 10th cycle, on further cycling the spinel structure stabilizes and exhibits good capacity retention corresponding to a columbic efficiency of 85% and a capacity fade of 0.4 mAh g^{-1} $cycle^{-1}$ for the last 10 cycles.

In the case of $LiFe_{0.25}Ni_{0.25}Mn_{1.5}O_4$, the cell delivers a discharge

Downloaded 30 Jun 2009 to 210.212.252.226. Redistribution subject to ECS license or copyright; see http://www.ecsdl.org/terms_use.jsp

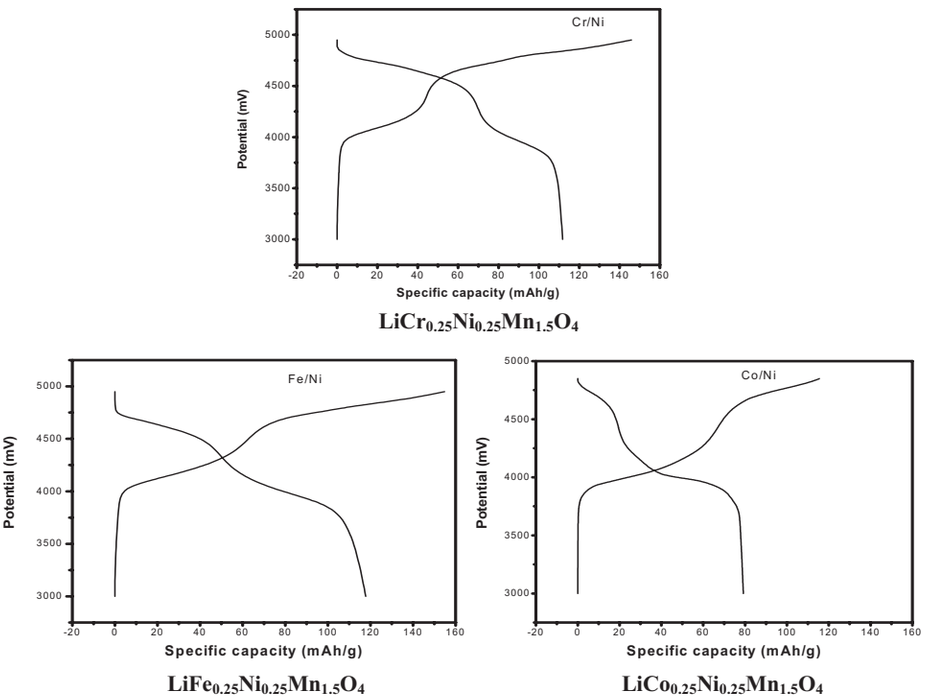

Figure 6. Charge–discharge behavior of $LiM_{0.25}Ni_{0.25}Mn_{1.5}O_4$ (M = Cr, Fe, and Co) samples calcined at 850°C.

capacity of 120 mAh g^{-1} during the 1st cycle against the charging capacity of 158 mAh g^{-1}. These cells exhibit a very low-capacity fade of 0.05 mAh g^{-1} $cycle^{-1}$ over the investigated 20 cycles. In the 20th cycle, the cell delivered 120 mAh g^{-1} as discharge capacity. These results are superior to the earlier studies by Fey et al.,[16] wherein Fe-doped spinel delivered only 117 mAh g^{-1} in the 1st cycle and 100 mAh g^{-1} in the 20th cycle. It is evident that $LiFe_{0.25}Ni_{0.25}Mn_{1.5}O_4$ compound exhibits high specific discharge capacity with good capacity retention with 84% columbic efficiency.

Similarly, in the case of $LiCo_{0.25}Ni_{0.25}Mn_{1.5}O_4$, the cell delivers discharge capacity of 80 mAh g^{-1} during the 1st cycle against the charging capacity of 120 mAh g^{-1}. The cell retains a discharge capacity of 60 mAh g^{-1} in the 20th cycle. Co/Ni-doped cells deliver better performance than the earlier reports by Rojas et al.,[31] wherein $LiNi_{0.05}Co_{0.9}Mn_{1.95}O_4$ delivered discharge capacity of 75 mAh g^{-1} in the 1st cycle and 50 mAh g^{-1} in the 20th cycle.

Among the investigated duo-doped spinels, Fe/Ni couple

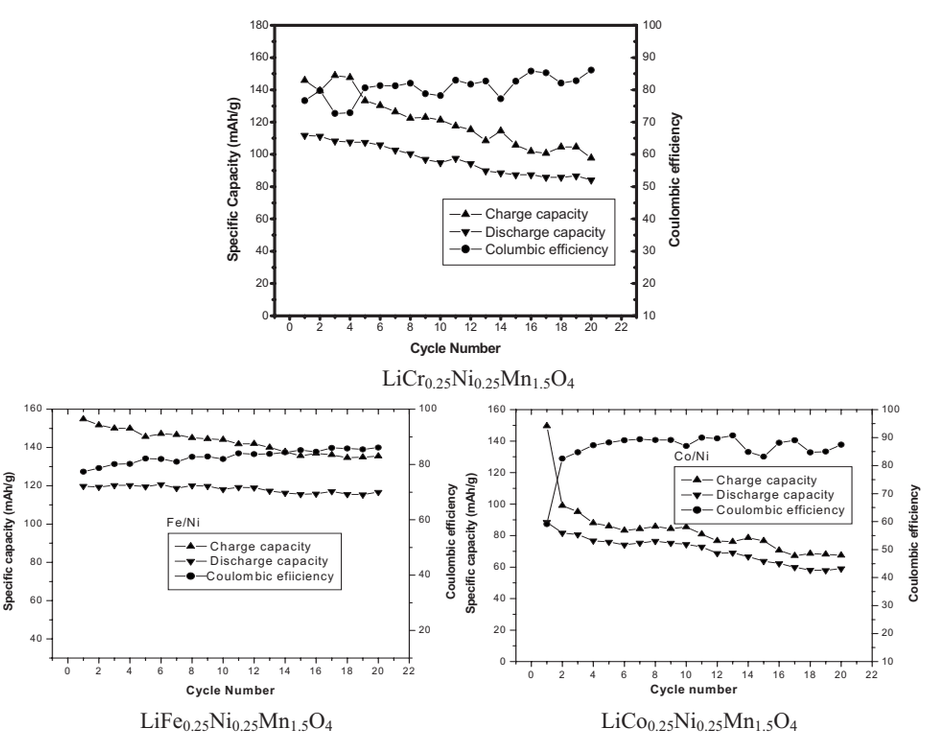

Figure 7. Cycling behavior of $LiM_{0.25}Ni_{0.25}Mn_{1.5}O_4$ (M = Cr, Fe, and Co) samples calcined at 850°C.

Downloaded 30 Jun 2009 to 210.212.252.226. Redistribution subject to ECS license or copyright; see http://www.ecsdl.org/terms_use.jsp

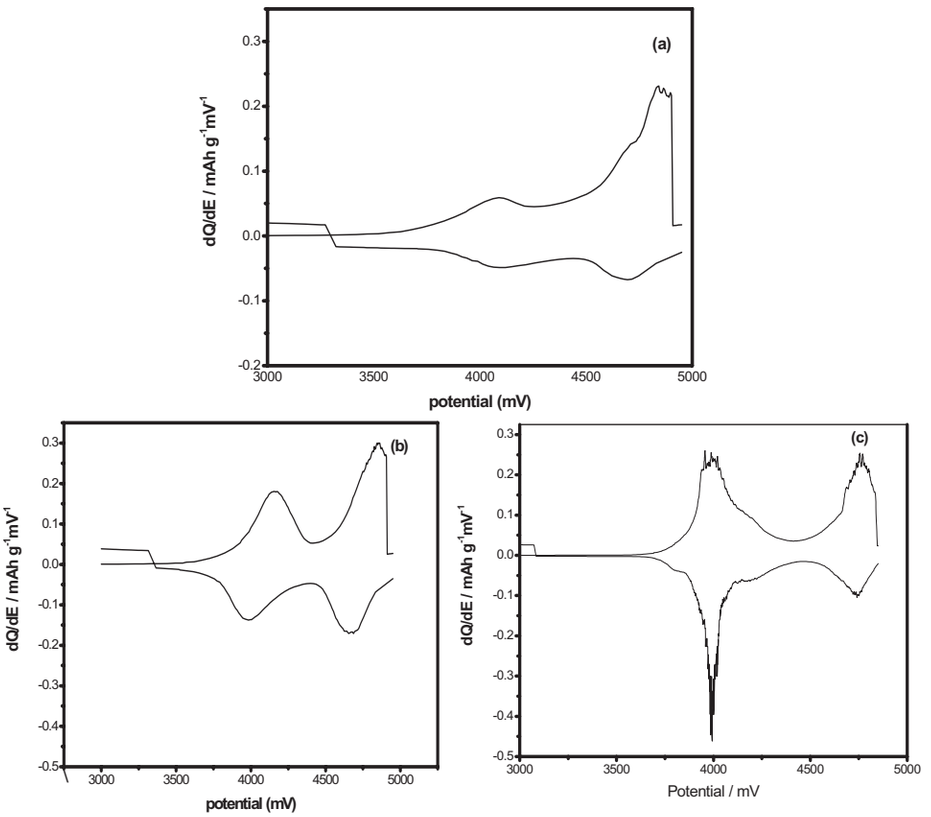

(a) $LiCr_{0.25}Ni_{0.25}Mn_{1.5}O_4$ (b) $LiFe_{0.25}Ni_{0.25}Mn_{1.5}O_4$ (c) $LiCo_{0.25}Ni_{0.25}Mn_{1.5}O_4$

Figure 8. Differential capacity curves of $LiM_{0.25}Ni_{0.25}Mn_{1.5}O_4$ (M = Cr, Fe, and Co) samples calcined at 850°C.

($LiFe_{0.25}Ni_{0.25}Mn_{1.5}O_4$) outperforms than the rest in terms of higher discharge capacity and capacity retention characteristics in the investigated 20 cycles. When comparing the ionic radii of the doped cations (Co: 0.745 Å, Cr: 0.52 Å, Fe: 0.645 Å, Ni: 0.69 Å), the near similar combination of Fe/Ni couple provides a corporate supporting attitude toward stabilizing the spinel structure over the repeated cycling and hence $LiFe_{0.25}Ni_{0.25}Mn_{1.5}O_4$ could be an attractive 5 V cathode material to use in lithium rechargeable batteries.

Differential capacity studies.— Figures 8a-c depict differential capacity curves drawn from the charge–discharge data of $LiM_{0.25}Ni_{0.25}Mn_{1.5}O_4$ (M = Cr, Fe, and Co) powders calcined at 850°C, respectively. It can be seen that the dQ/dE curves reflect the redox behavior of the cycling process. The oxidative peaks are representing the lithium extraction process, and the reductive peaks indicate lithium insertion step. In all cases, the dQ/dE curves depict a two-stage reaction in both the oxidative and reductive sides. These correspond to the redox reactions of two cationic dopants. It is evident from the figures that in the case of the Fe/Ni couple, the reaction proceeds in an orderly way. The peak potentials and the intensity corresponding to the oxidation and reduction process are equally prospective, indicating that the reactions are of first order in nature. There is no shift in peak potentials observed for both the lithium insertion and extraction process, corroborating the fact that the structural environment for the lithium-ion transit is more congenial and efficient, further establishing the fact that $LiFe_{0.25}Ni_{0.25}Mn_{1.5}O_4$ could be an attractive cathode material to use in lithium rechargeable batteries.

Figure 8a lucidly depicts the differential capacity curve of the $LiCr_{0.25}Ni_{0.25}Mn_{1.5}O_4$ calcined at 850°C. It is evident that two indistinct anodic peaks are observed at ~4.0 and 4.8 V, which corresponds to this process at the 8a tetrahedral sites associated with Mn^{3+}/Mn^{4+}, Cr^{3+}/Cr^{4+}, and Ni^{2+}/Ni^{4+}, and cathodic peaks between 4.7 and 4.0 V are attributed to Ni^{4+}/Ni^{2+}, Mn^{4+}/Mn^{3+}, and Cr^{4+}/Cr^{3+}. In the case of $LiFe_{0.25}Ni_{0.25}Mn_{1.5}O_4$ (Fig. 8b) compounds, it reveals two well-defined anodic peaks, one peak at 4.1 V assigned to Mn^{3+}/Mn^{4+}, and the peak at 4.8 V corresponds to Fe^{3+}/Fe^{4+} and Ni^{2+}/Ni^{4+}, and two cathodic peaks between 4.7 and 3.9, which are attributed to Fe^{4+}/Fe^{3+}, Ni^{4+}/Ni^{2+}, and Mn^{4+}/Mn^{3+}. Also, the $LiCo_{0.25}Ni_{0.25}Mn_{1.5}O_4$ (Fig. 8c) compound clearly illustrates that two broad anodic peaks (Mn^{3+}/Mn^{4+}, Co^{2+}/Co^{3+}, and Ni^{2+}/Ni^{4+}), and two cathodic peaks with a very sharp one corresponding to Mn^{4+}/Mn^{3+}, Co^{3+}/Co^{2+}, and Ni^{4+}/Ni^{2+}. From the above preliminary investigations, it is clearly understood that the $LiFe_{0.25}Ni_{0.25}Mn_{1.5}O_4$ compound seems to be an attractive candidate to enhance the better electrochemical reversibility than other dopants.

CV studies.— A typical cyclic voltammetric curve obtained for $LiFe_{0.25}Ni_{0.25}Mn_{1.5}O_4$ is depicted in Fig. 9. As observed, no peak is ~3 V and it can be said that no manganese is present in the 3^+ state[32] in the synthesized material. It is clear from the figure that the two major oxidation peaks are observed at around 4.1 and 4.8 V, and the two major reduction peaks are observed at around 3.95 and 4.55 V, respectively, and this is representative of the lithium deintercalation and reintercalation processes. These peaks are also signatures of cubic spinel compounds and indicate perfect reversibility. The peaks at ~4.1 V could be assigned to electrochemical oxidation of manganese ions, and the peaks at ~4.8 V could be assignable to oxidation of Ni and Fe. Similarly, the two peaks observed around 3.9 and 4.6 V indicate the reduction processes of manganese and doped ions.

Conclusions

Glycine-assisted sol–gel synthesized multiple-doped spinels $LiM_{0.25}Ni_{0.25}Mn_{1.5}O_4$ (M = Cr, Fe, and Co) have been studied as

Downloaded 30 Jun 2009 to 210.212.252.226. Redistribution subject to ECS license or copyright; see http://www.ecsdl.org/terms_use.jsp

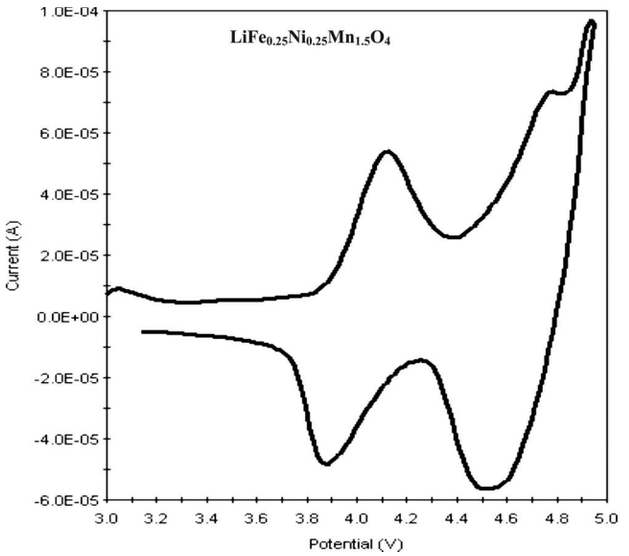

Figure 9. Cyclic voltammogram of $LiFe_{0.25}Ni_{0.25}Mn_{1.5}O_4$ electrode.

possible 5 V cathode materials. TG/DTA curves of undoped spinel and $LiM_{0.25}Ni_{0.25}Mn_{1.5}O_4$ (M = Cr, Fe, and Co) precursors depict the nature of the thermal process and the formation temperature of the compound. XRD patterns of doped spinels exhibit a high degree of crystallinity with better phase purity. SEM images of $LiM_{0.25}Ni_{0.25}Mn_{1.5}O_4$ (M = Cr, Fe, and Co) powders calcined at 850°C depict the grain morphology. XPS studies of $LiFe_{0.25}Ni_{0.25}Mn_{1.5}O_4$ powder indicate that the metal species, namely Ni, Fe, and Mn, are in 2^+, 3^+, and 4^+ oxidation states, respectively. Among the investigated duo-doped spinels, the Fe/Ni couple ($LiFe_{0.25}Ni_{0.25}Mn_{1.5}O_4$) outperforms the rest in terms of higher discharge capacity (120 mAh g^{-1}) and capacity retention characteristics (low-capacity fade of 0.05 mAh g^{-1} $cycle^{-1}$) in the investigated 20 cycles. Differential capacity curves drawn from the charge–discharge data of $LiM_{0.25}Ni_{0.25}Mn_{1.5}O_4$ (M = Cr, Fe, and Co) cells disclose the nature of the redox process and reiterate the efficient transit of lithium ions into the spinel structure in the case of $LiFe_{0.25}Ni_{0.25}Mn_{1.5}O_4$, and confirm the fact that the said material could be an attractive cathode material to use in lithium rechargeable batteries. Furthermore, the cyclic voltammetric curve obtained for $LiFe_{0.25}Ni_{0.25}Mn_{1.5}O_4$ also substantiates the results.

Acknowledgment

The authors thank the Department of Science and Technology, India, for support under the DST-JST project no. JAP/SCP-011.

Kyushu University assisted in meeting the publication costs of this article.

References

1. J. H. Kim, C. S. Yoon, and Y. K. Sun, *Electrochem. Solid-State Lett.*, **7**, A216 (2004).
2. M. Wohlfahrt-Mehrens, C. Vogler, and J. Garche, *J. Power Sources*, **127**, 58 (2004).
3. M. M. Thackeray, Y. Shao-Horn, A. J. Kahaian, K. D. Kepler, E. Skinner, J. T. Vaughey, and S. A. Hackney, *Electrochem. Solid-State Lett.*, **1**, 7 (1998).
4. R. J. Gummow, A. de Kock, and M. M. Thackeray, *Solid State Ionics*, **69**, 67 (1994).
5. D. H. Jang, J. Y. Shin, and S. M. Oh, *J. Electrochem. Soc.*, **143**, 2204 (1996).
6. S. T. Myung, H. T. Chung, S. Komaba, N. Kumagai, and H. B. Gu, *J. Power Sources*, **90**, 103 (2000).
7. J. M. Tarascon, W. R. McKinnon, F. Coowar, T. N. Bowmer, G. Amatucci, and D. Guyomard, *J. Electrochem. Soc.*, **141**, 1421 (1994).
8. T. Ohzuku, S. Takeda, and M. Iwanaga, *J. Power Sources*, **81–82**, 90 (1999).
9. J. H. Lee, J. K. Hong, D. H. Jang, Y. K. Sun, and S. M. Oh, *J. Power Sources*, **89**, 7 (2000).
10. A. D. Robertson, S. H. Lu, and W. F. Howard, *J. Electrochem. Soc.*, **144**, 3505 (1997).
11. Q. Zhong, A. Bonakdarpour, M. Zhang, Y. Gao, and J. R. Dahn, *J. Electrochem. Soc.*, **144**, 205 (1997).
12. T. A. Arunkumar and A. Manthiram, *Electrochim. Acta*, **50**, 5568 (2005).
13. Y. S. Lee, Y. K. Sun, S. Ota, T. Miyashita, and M. Yoshio, *Electrochem. Commun.*, **4**, 989 (2002).
14. L. J. Fu, H. Liu, C. Li, Y. P. Wu, E. Rahm, R. Holze, and H. Q. Wu, *Prog. Mater. Sci.*, **50**, 881 (2005).
15. S. H. Oh, K. Y. Chung, S. H. Jeon, C. S. Kim, W. I. Cho, and B. W. Cho, *J. Alloys Compd.*, In press. [DOI: 10.1016/j.jallcom.2008.01.097]
16. G. T. K. Fey, C. Zhang Lu, and T. Prem Kumar, *J. Power Sources*, **115**, 332 (2003).
17. B. J. Hwang, R. Santhanam, and S. G. Hu, *J. Power Sources*, **108**, 250 (2002).
18. Y. W. Tsai, R. Santhanam, B. J. Hwang, S. K. Hu, and H. S. Sheu, *J. Power Sources*, **119**, 701 (2003).
19. G. Kumar, H. Schlorb, and D. Rahner, *Mater. Chem. Phys.*, **70**, 117 (2001).
20. R. Thirunakaran, A. Sivashanmugam, S. Gopukumar, C. W. Dunnill, and D. H. Gregory, *J. Phys. Chem. Solids*, **69**, 2082 (2008).
21. R. Thirunakaran, K.-T. Kim, Y.-M. Kang, C.-Y. Seo, and J.-Y. Lee, *J. Power Sources*, **137**, 100 (2004).
22. T. Ohzuku, K. Ariyoshi, S. Takeda, and Y. Sakai, *Electrochim. Acta*, **46**, 2327 (2001).
23. M. M. Thackeray, *Prog. Solid State Chem.*, **25**, 1 (1997).
24. M. M. Thackeray, W. I. F. David, P. G. Bruce, and J. B. Goodenough, *Mater. Res. Bull.*, **18**, 461 (1983).
25. A. F. Carley, S. D. Jackson, J. N. O'Shea, and M. W. Roberts, *Surf. Sci.*, **440**, L868 (1999).
26. K. Amine, H. Tukamoto, H. Yasuda, and Y. Fujita, *J. Electrochem. Soc.*, **143**, 1607 (1996).
27. S. Gopukumar, K. Y. Chung, and K. B. Kim, *Electrochim. Acta*, **49**, 803 (2004).
28. S. H. Kang, J. Kim, M. E. Stoll, D. Abraham, Y. K. Sun, and K. Amine, *J. Power Sources*, **112**, 41 (2002).
29. L. Hernan, J. Morales, L. Sanchez, E. Rodriguez Castellon, and M. A. G. Aranda, *J. Mater. Chem.*, **12**, 734 (2002).
30. G. Liu, H. Xie, L. Liu, X. Kang, Y. Tian, and Y. Zhai, *Mater. Res. Bull.*, **42**, 1955 (2007).
31. R. M. Rojas, J. M. Amarilla, L. Pascual, J. M. Rojo, D. Kovacheva, and K. Petrov, *J. Power Sources*, **160**, 529 (2006).
32. J. M. Paulsen, C. L. Thomas, and J. R. Dahn, *J. Electrochem. Soc.*, **147**, 861 (2000).

Downloaded 30 Jun 2009 to 210.212.252.226. Redistribution subject to ECS license or copyright; see http://www.ecsdl.org/terms_use.jsp